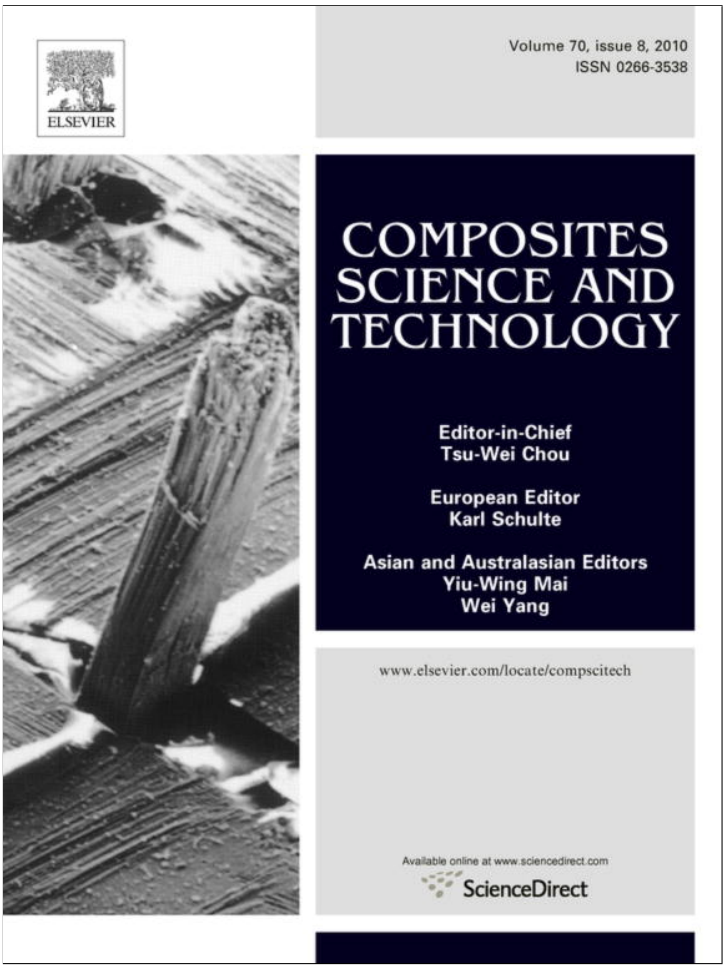

Composites Science and Technology 70 (2010) 1199–1206

Contents lists available at ScienceDirect

Composites Science and Technology

journal homepage: www.elsevier.com/locate/compscitech

Multi-walled carbon nanotubes reinforced Al_2O_3 nanocomposites: Mechanical properties and interfacial investigations

I. Ahmad [a], M. Unwin [b], H. Cao [c], H. Chen [c], H. Zhao [c], A. Kennedy [a], Y.Q. Zhu [a,*]

[a] Division of Materials, Mechanics and Structure, Faculty of Engineering, The University of Nottingham, University Park, NG7 2RD, UK
[b] School of Electrical and Electronic Engineering, Faculty of Engineering, The University of Nottingham, Nottingham NG7 2RD, UK
[c] Department of Materials Science and Engineering, China University of Mining and Technology, D11 Xueyuan Lu, Beijing 100083, China

ARTICLE INFO

Article history:
Received 12 January 2010
Received in revised form 3 March 2010
Accepted 14 March 2010
Available online 18 March 2010

Keywords:
A. Carbon nanotubes
A. Nanocomposites
A. Ceramic–matrix composites
B. Fracture toughness
B. Interface

ABSTRACT

Well-dispersed multi-walled carbon nanotubes (CNTs) reinforced Al_2O_3 nanocomposites were successfully fabricated by hot-pressing. The resulting promising improvements in fracture toughness, by 94% and 65% with 2 and 5 wt.% CNTs addition respectively, compared with monolithic Al_2O_3, were attributed to the good dispersion of CNTs within the matrix, crack-bridging by CNTs and strong interfacial connections between the CNTs and the matrix. The interfacial phase characteristics between CNTs and Al_2O_3 were investigated via combined techniques. It is believed that a possible aluminium oxy-carbide as the primary interfacial phase was produced via a localized carbothermal reduction process. This interface phase presumably has good chemical compatibility and strong connections with both CNTs and the matrix and led nanocomposites to higher fracture toughness.

1. Introduction

Extreme brittle nature of ceramics restricted them from numerous advanced structural applications [1]. In order to overcome the toughness problem, incorporation of particulates (ceramics, pure metal) and long/short fibres (glass, carbon), as a second phase, into ceramics matrices to make composites is an eminent practice for decades [2–4]. Recent advances in nanomaterials, in particular carbon nanotubes (CNTs), have offered exciting potentials for utilising these novel materials for the production of toughened polycrystalline ceramics [5]. Single-walled and multi-walled CNTs show excellent mechanical, electrical and thermal properties therefore, it is postulated that the ceramics–CNT nanocomposites will demonstrate multifunctional properties in addition to the higher mechanical properties [6,7]. Among ceramics, Al_2O_3 has a wide range of applications in medical, aerospace and automobile industries, which arise from its superior hardness, chemical inertness and electrical/thermal insulation properties but deprived toughness is still a main issue [8,9]. In reported cases, reinforcing by CNTs (both single and multi-walled) has upgraded the Al_2O_3 toughness however, wide scattered and highly debatable (reproducibility and toughening mechanism) results were found, some of the variations may purely arise from different testing techniques used, such as single edged pre-cracked beam (SEPB), single edged notched beam (SENB), direct crack measurement (DCM) [10–21]. Physically, the presence of CNTs in an Al_2O_3 matrix is likely to exhibit two major functions: (a) decreasing the sintered densities of composite due to their existence at the grain boundaries, which hinders achieving full density of the nanocomposite; and (b) sharply reducing the grain size by restricting the grain from further growth [22,23]. Mechanically, the improvement in properties is due to bridging the crack surfaces by CNTs during crack propagation under applied load and CNT pullout mechanism [13–24]. These strengthening/toughening phenomena in CNTs reinforced nanocomposites depend strongly on the interfacial bonding between CNTs and the matrix. Indeed, a good interface can transfer the load between CNTs and the matrix [24]. Therefore, understanding of the microstructure down to the atomic level is imperative in order to improve the properties of ceramics based composites. For example, in conventional fibre reinforced ceramics composites, the interface between fibre and matrix is important and controls the various micro-mechanisms, which act as energy dissipative processes during mechanical loading, such as fibre debonding, fibre pullout and crack-bridging. In fact, interface is a complex layered transitional region between fibre and matrix therefore, controlling the interface chemistry and tailoring smart microstructures are essential steps in the fabrication of novel composites with high fracture toughness and fracture strength [25]. However, the understanding of the nanostructured characteristics of the composites and the interfacial phenomena between CNTs and the Al_2O_3 matrix is far from satisfactory [24–26]. In this context, the manufacturing

* Corresponding author.
E-mail address: Yanqiu.zhu@nottingham.ac.uk (Y.Q. Zhu).

0266-3538/$ - see front matter © 2010 Elsevier Ltd. All rights reserved.
doi:10.1016/j.compscitech.2010.03.007

of hot-pressed Al_2O_3–CNT nanocomposites with a good dispersion of CNTs is described. The mechanical properties, micro/nanostructural analysis and interface investigations of the nanocomposites are presented.

2. Experimental procedure

Multi-walled CNTs having an outer diameter of ~40 nm (Tsinghua University, Beijing, China) were first chemically processed with a H_2SO_4–HNO_3 solution, to thoroughly remove the metallic catalyst. They were then dispersed into an aqueous solution containing a small quantity (<2 wt.% of CNTs) of sodium dodycyle sulphate (SDS, Sigma–Aldrich, UK) surfactant, with the help of ultrasonic probe sonication for 30 min (Sonic Processor D-100-20, Sonic system, UK). The CNT slurry was incubated for 2 weeks, to allow the surfactant to thoroughly adsorb onto the CNT surfaces. δ-Al_2O_3 nanoparticles with a mean size of 40 nm (Sigma Aldrich, UK) was then added and sonicated again for 120 min. After drying, the mixture was hot-pressed in a graphite die (University of Mining and Technology, Beijing, China) under a pressure of 40 MPa at 1600 °C for 60 min, at a heating rate of 10 °C/min under vacuum (6.2×10^{-2} Pa). Diameter discs (32 mm) of the nanocomposites were produced. Monolithic Al_2O_3 was also hot-pressed under the same conditions for comparison. Densities of the sintered samples were measured by Archimedes method in distilled water and relative densities were calculated by dividing the measured densities by theoretical densities, and for this purpose 1.8 g/cm^3 and 3.9 g/cm^3 were considered the theoretical densities for CNT and monolithic Al_2O_3, respectively [18,27]. Microhardness testing was carried out at 9.8 N loads for 15 s (M-400 hardness tester, LECO, Japan). The flexural strength (σ_f) was measured by three-point bending method, and the size of specimens was 25 mm (length) × 2 mm (breadth) × 2.5 mm (height). The bending span and the load speed for the strength were 20 mm and 0.5 mm/min respectively. The fracture toughness (K_{IC}) was evaluated by direct crack measurement (DCM) technique and single edge notched beam (SENB) method. In DCM technique, the fracture toughness was obtained by measuring the crack length from the indentation centre using scanning electron microscopy, SEM, (Philips/FEI XL30-JEOL 6400; Philips/FEI XL30 FEG-ESEM), in combination with computer software ImageJ (Image Processing and Analysis in Java) [28]. For SENB method, three samples were prepared with identical dimension using similar specimen preparation procedures as adopted for the flexural strength samples [29]. However, a notch was produced at the centre of the specimens, using a resin-bonded diamond blade. Three point bend test was performed on the notched specimens, at the loading speed of 0.05 mm/min and fracture toughness was calculated. A standard ultrasonic pulse-echo technique was used to assess the modulus of elasticity of the samples. During the pulse-echo measurements, the time-of-flight velocities for both compression and shear wave propagating through the samples were recorded. Compression measurements were made using 20 MHz centre frequency, ∅ 6 mm contact transducers (TMP-3, Sonatest, UK). The equivalent shear measurements were performed with a 10 MHz centre frequency, ∅ 10 mm contact transducer (V221-BA, Panametrics, USA). Appropriate couplant materials were used in each case to ensure optimum contact between the samples and transducers. From the velocities measurements, modulus of elasticity of monolithic Al_2O_3 and Al_2O_3–CNT nanocomposites were then calculated [30].

Thermal investigations of the samples were carried out using a SDTQ600 (TA Instruments, USA). During the thermal testing, samples were heated in Ar up to 1400 °C at a heating rate of 20 °C/min and the evaluation of CO was simultaneously recorded using an attached HPR20-QIC atmospheric gas analyser (Hiden Analytical, UK). Although kinetically this atmosphere pressure analysis is different from the hot-press conditions, the thermodynamic and reaction products may somehow be analogue to those formed in the hot-pressed samples. Structural features from the fractured samples were assessed by SEM. X-ray diffraction (XRD) using Cu kα radiation was performed (Siemens D500 and Bruker D8 Advanced X-ray Differactometer) to identify the crystalline phase features of the nanocomposites. SEM and XRD techniques were also employed to determine the grain size of the samples. Transmission electron microscopy (TEM, JEOL 2000 FX and 2100 F) were used to characterise the interfacial structures in the nanocomposite. TEM samples were prepared by deep corrosive etching using NaOH for 2 weeks followed by a thorough rinsing with distilled water in order to remove traces of NaOH. The clean samples were dispersed in acetone and then transferred onto a holey carbon film supported on a copper grid, for observation. This easy etching technique allows for the partly removal of Al_2O_3, by forming soluble $NaAlO_2$, whilst keeping the CNTs intact. In addition to chemical etching method, focused ion beam (FIB) milling technique (FEI Quanta200 3D Dual Beam FIB/SEM) was also utilised to prepare thin samples for TEM investigations. In FIB milling, selected area of nanocomposite sample was milled using Ge ions and then the milled section was detached from the bulk sample by welding it with special probe. Both techniques produced good quality samples for TEM analysis.

3. Results and discussion

3.1. Results

TEM images shown in Fig. 1 display the morphology and surface features of the CNTs used in this research. The surface of the CNTs is not smooth, and a hollow core and numerous graphitic layers of the CNTs are clearly visible, although the layers are not concentrical on a long distance and many compartments exist, which is a typical feature of CNTs made by chemical vapour deposition. After consolidation of the CNT/Al_2O_3 nanoparticles mixture using hot-pressing, the fractured sample surfaces of the sintered nanocomposites revealed good dispersion of CNTs within the matrix (Fig. 2b and c). Fig. 2d clearly shows the individually dispersed CNTs within the Al_2O_3 matrix. A relative density of 99.6% has been achieved for monolithic Al_2O_3, as shown in Table 1. However, 0.5% and 3.4% reductions in the relative density were observed for nanocomposites containing 2 and 5 wt.% CNTs, respectively. Regarding mechanical properties, a 13% increase in hardness at 2 wt.% CNTs addition and a slight reduction by 7% at 5 wt.% CNTs addition were observed for the nanocomposite, as summarised in Table 1. The table also shows a 41% and 47% improvement in the fracture toughness assessed by the DCM method for composites containing 2 and

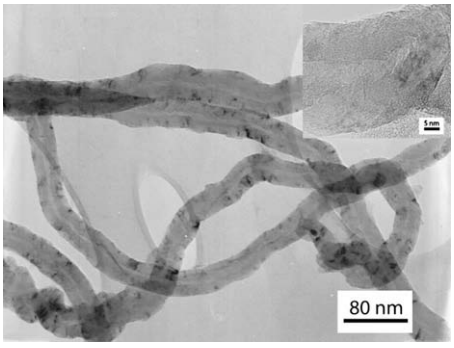

Fig. 1. TEM image of the pristine CNTs and high-resolution TEM image of a CNT (inset).

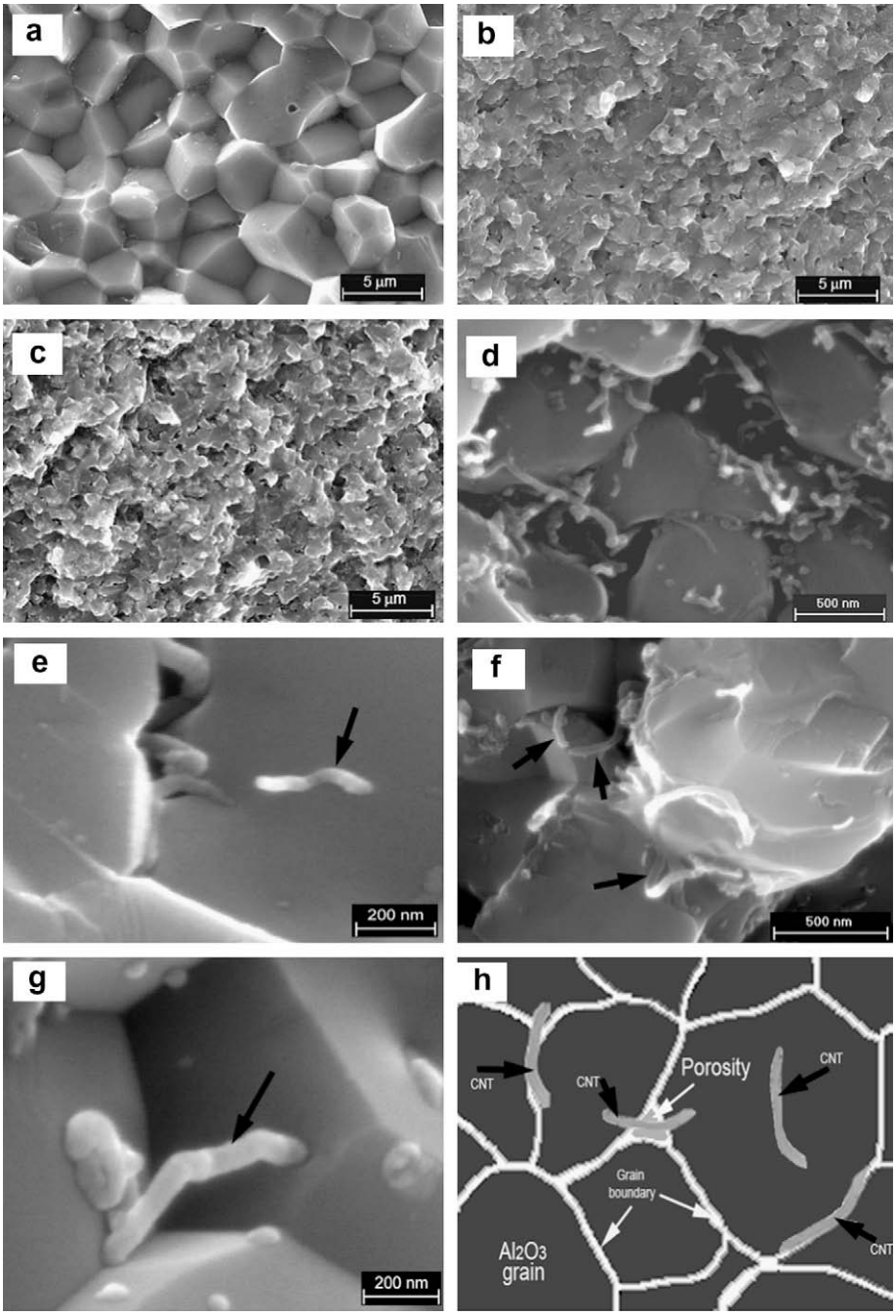

Fig. 2. SEM images of the fractured surface of: (a) monolithic Al_2O_3, (b) Al_2O_3–2 wt.% CNTs, (c) Al_2O_3–5 wt.% CNTs, (d) CNTs dispersion within matrix at high magnification and location of CNTs (black arrow) in nanocomposite, (e) within grain, (f) at grain boundary, (g) CNTs (black arrows) bridging the grains and (h) a schematic of CNTs' favourable locations (black arrows) within the Al_2O_3 matrix.

Table 1
Properties of Al_2O_3–CNT nanocomposites.

Material	Measured density (g/cm^3)	Relative density (%)	Grain size (μm)	Hardness (HV) (GPa)	Fracture toughness (K_{IC}) (MPa $m^{1/2}$)		Flexural strength (σ_f) (MPa)
					SENB method	DCM method	
Al_2O_3 (monolithic)	3.88 ± 0.01	99.6	1.3 ± 0.2	16 ± 0.4	3.5 ± 0.2	3.0 ± 0. 2	357 ± 27
Al_2O_3–2 wt.% MWCNTs	3.82 ± 0.02	99.1	0.4 ± 0.1	18 ± 0.3	6.8 ± 0.3	4.3 ± 0.3	380 ± 18
Al_2O_3–5 wt.% MWCNTs	3.65 ± 0.02	96.2	0.3 ± 0.1	15 ± 0.5	5.8 ± 0.2	4.5 ± 0.2	280 ± 7

5 wt.% CNTs respectively, as compared to the monolithic Al_2O_3. Most recently, there is a technical debate regarding the toughness testing methods for ceramics. It is considered that the decades old DCM technique is unreliable for assessing ceramic fracture toughness and that this technique could be fundamentally flawed, although numerous reports were based on it [19–21,31].

Nevertheless, the standard SENB method was also employed in this context. Interestingly, 94% and 65% increases in fracture toughness were obtained for identical samples with 2 and 5 wt.% CNTs. This result seems to reinforce the current debate and will be discussed later. For the flexural strength, marginal improvement was observed for 2 wt.% CNTs, and a 20% drop for 5 wt.% CNTs, when compared with the unreinforced Al_2O_3.

3.2. Densification and structural features

The density reduction of the Al_2O_3–CNT nanocomposites with increasing CNT content in the matrix is a well-documented phenomenon [12–18,32,34]. The decrease can be associated with the presence of CNTs heaps, Fig. 4b, and the special densification mechanism. Well-dispersed CNTs lead to nanocomposites with higher sintered densities while CNT heaps result in lower densities [31]. Generally, the elimination of pores and mass transportation through bulk diffusion are two basic factors that determine the final density during the sintering of Al_2O_3 [33]. It is believed that the addition of CNTs, even if they are well-dispersed, has adverse effects on the two important sintering parameters. Existence of CNTs at grain boundaries prevented the grains closing during densification and offered fine grains in the final nanocomposites by grain pinning [32]. In addition to grain size reduction, existence of CNTs in matrix changed the fracture mode from inter-granular fracture in monolithic Al_2O_3 (Fig. 2a) to trans-granular fracture in the nanocomposites, as exhibited in Fig. 2b and c. The morphology of the fractured surface of monolithic Al_2O_3 has revealed clearly the edge and corner fractural feature, which denotes the inter-granular fracture mode and conversely, a blurry and glaze-like morphology is indicative of the trans-granular mode of fracture caused by the CNTs [23]. The fracture mode change is more apparent at higher CNT contents, as shown in Fig. 2b. This shows that the CNTs, as second phase, are responsible for altering fracture mode, as previously reported [35].

3.3. Mechanical properties

Table 1 indicates that the addition of CNTs significantly affected the density, grain size and offered variation in the overall mechanical properties, in particular the fracture toughness, hardness and flexural strength. Marginal improvement in hardness and flexural strength at 2 wt.% CNT additions can be associated with the good dispersion of CNTs and high nanocomposite densities. However, significant reduction in hardness and flexural strength of the nanocomposite containing 5 wt.% CNTs can be justified with the

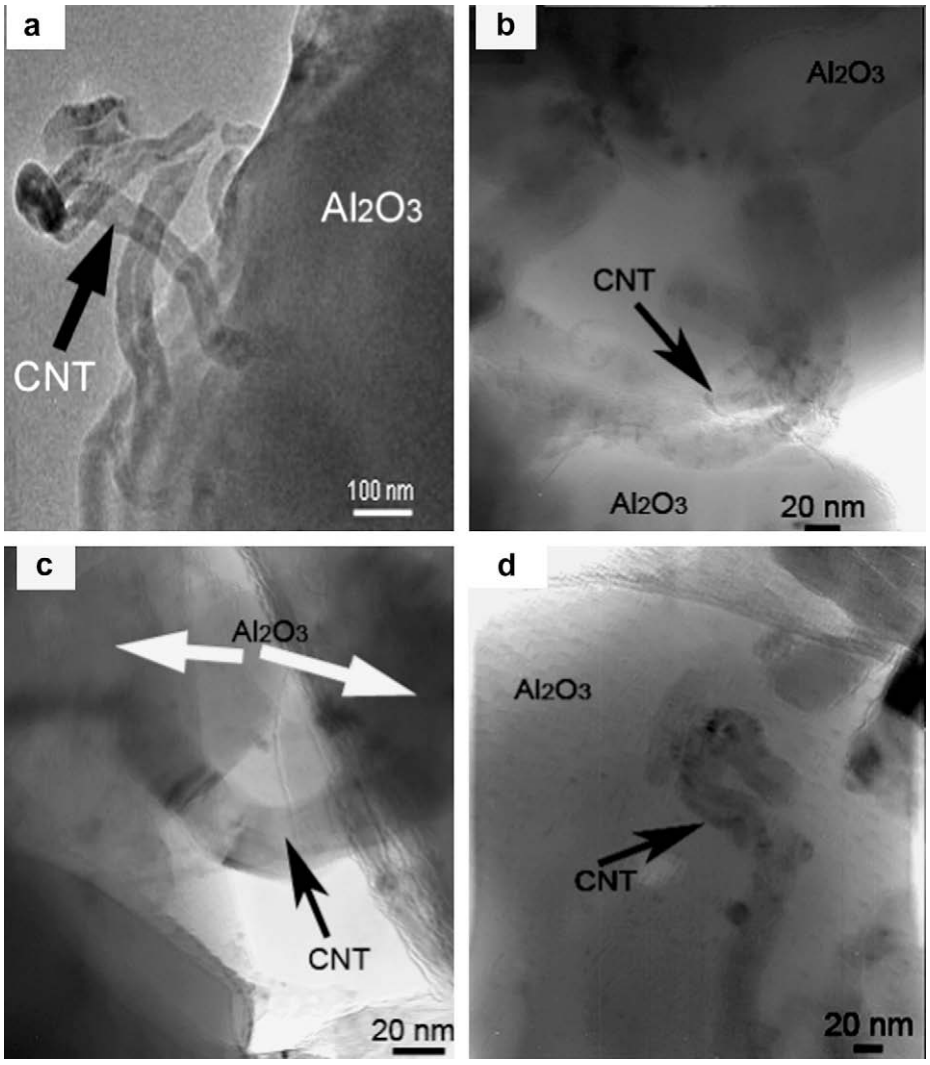

Fig. 3. TEM images exhibiting the Al_2O_3–CNT interactions: (a) CNTs (black arrow) showing their morphology in nanocomposite (FIB milling sample), (b) CNT exist at grain boundary, (c) in porosity and (d) embedded within a single Al_2O_3 grain (corrosion etching sample).

difficulties in achieving good dispersion for CNTs, differences in densification as a function of CNT additions and the presence of elongated pores in microstructures, as already proposed [23]. However, the 94% and 65% improvement in toughness at 2 wt.% and 5 wt.% of CNT additions, respectively, cannot be correlated fully with these proposed features. The evidence provided so far by such physical and structural features is not enough for claiming the reinforcing effect. The understanding of microstructure down to atomic level is imperative. In this context, the interface was explored using combined techniques to assess the bonding strength and possible chemical reactions occurred at the interface during severe fabrication processing conditions of elevated temperatures and high pressures. Combined SEM and TEM investigations at higher magnification revealed detailed features of CNTs interactions with the Al_2O_3 matrix, as shown in Figs. 2 and 3. CNTs can be embedded inside an Al_2O_3 grain, acting as a barrier for crack propagation, as demonstrated in Fig. 2e. Furthermore, CNTs can be seen between grain boundaries in Fig. 2f. In addition, CNTs can form a bridge between Al_2O_3 grains (Fig. 2g) which help to improve the crack resistance. On the basis of these observations, we have identified the favourable sites where CNTs are often presented within the matrix, as illustrated in Fig. 2h. TEM investigations further confirmed that CNTs occupied the same sites, Fig. 3b–d, as observed in SEM studies.

Large and small CNTs pullout lengths in Fig. 4a indicate that conventional pullout toughening mechanism is functional in nanocomposite and is likely operative at grain boundaries, where a weak matrix/CNTs interface can be expected due to the CNTs accumulation. During matrix cracking, the cracked surface are bridged by the CNTs, which can be elastically deformed having both end firmly attached with the matrix. Therefore, energy dissipation mechanism, which is operative during nanocomposite fracture, can be attributed with the work done by the elastic extension of CNTs over a distance at either end of CNTs [36]. However, to exploit the elastic property of CNTs, a strong interfacial connection at Al_2O_3/CNTs interface is vital.

3.4. Interface structures

Fractographic details of the nanocomposites are helpful in understanding and assessing the interfacial bonding strength between the matrix and CNTs, to some extent. Close inspections of the pullout CNTs in the fractured surface of nanocomposites (Fig. 4a), have revealed that the CNTs resisted in pulling out of the Al_2O_3 matrix, which can be associated with proper bonding. In this regard, the surface roughness feature of the CNT surface could be interesting. From Fig. 1, the high surface roughness of the CNTs could result in two potential advantages: chemically reactive and physically difficult to slide out of the matrix, compared with a smooth surface. The former could help to improve the interfacial bonding with the matrix and the latter can pose much larger friction forces to stop the CNT pullout. High-resolution TEM studies further revealed detailed interfacial features of the nanocomposites. Fig. 5a and b depicts three distinct areas at the CNT–Al_2O_3 interface, and Al_2O_3 was identified by its fringe spacing of 0.26 nm and 0.34 nm corresponding to the (1 0 4) and (0 1 2) planes, respectively. Based on the curvature and bending features, CNTs can also be identified according to the 0.34 nm fringe separation which corresponds to the (0 0 2) graphitic plane. At the junction of Al_2O_3–CNT, a thin layer is clearly visible, with an undefined crystalline pattern, being neither Al_2O_3 nor CNTs.

3.5. Interfacial reaction

In order to obtain an insightful understanding of the bonding between the Al_2O_3 and CNTs, thermal analyses of monolithic Al_2O_3 and mixed powders, containing 2 and 5 wt.% CNTs, were carried out using TGA and DTA (differential thermal analysis), and the results are shown in Fig. 6. TGA results show an initial weight loss of 1.3% below 400 °C, which includes a possible loss of moisture absorbed from air and organic material added during processing stage. Monolithic Al_2O_3 exhibited a minimal weight loss ~0.5% between 400 °C to 1400 °C, whilst 1.05% and 1.31% weight loss were recorded for samples containing 2 and 5 wt.% CNTs respectively, for the same temperature range. DTA profile exhibits an exothermic peak at ~1242 °C which was assigned to reaction between CNTs and Al_2O_3, as illustrated in Fig. 6a(ii and iii), and no such peak is visible in Fig. 6a(i) for monolithic Al_2O_3. The mass spectrum of Al_2O_3–CNT nanocomposite shows the presence of increasing CO pressure, but not for the monolithic Al_2O_3 during the whole heating regime. The CO pressure recorded for the composite is significantly higher than that of the monolithic Al_2O_3, which agrees well

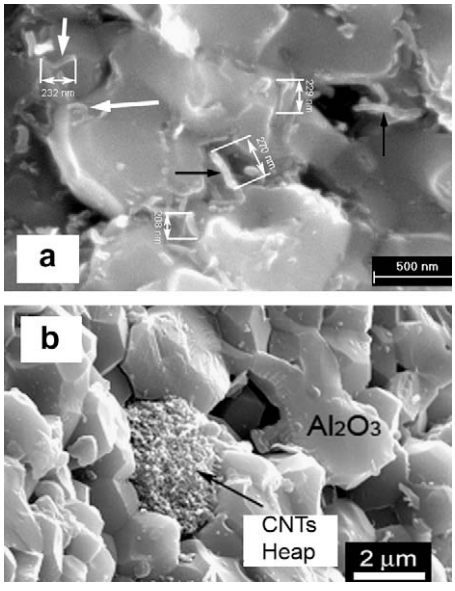

Fig. 4. Fractured surfaces of Al_2O_3–CNT nanocomposite: (a) CNT large pullout (black arrows show CNTs at grain boundary), small pullout and (b) a CNT heap in the matrix.

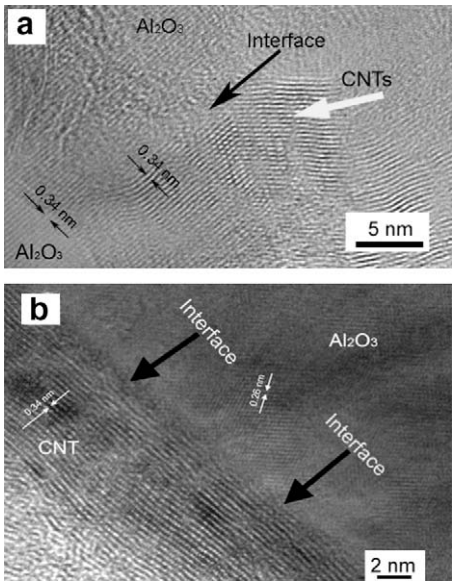

Fig. 5. (a and b) High-resolution TEM images of the Al_2O_3–CNT nanocomposite interface (FIB milling sample).

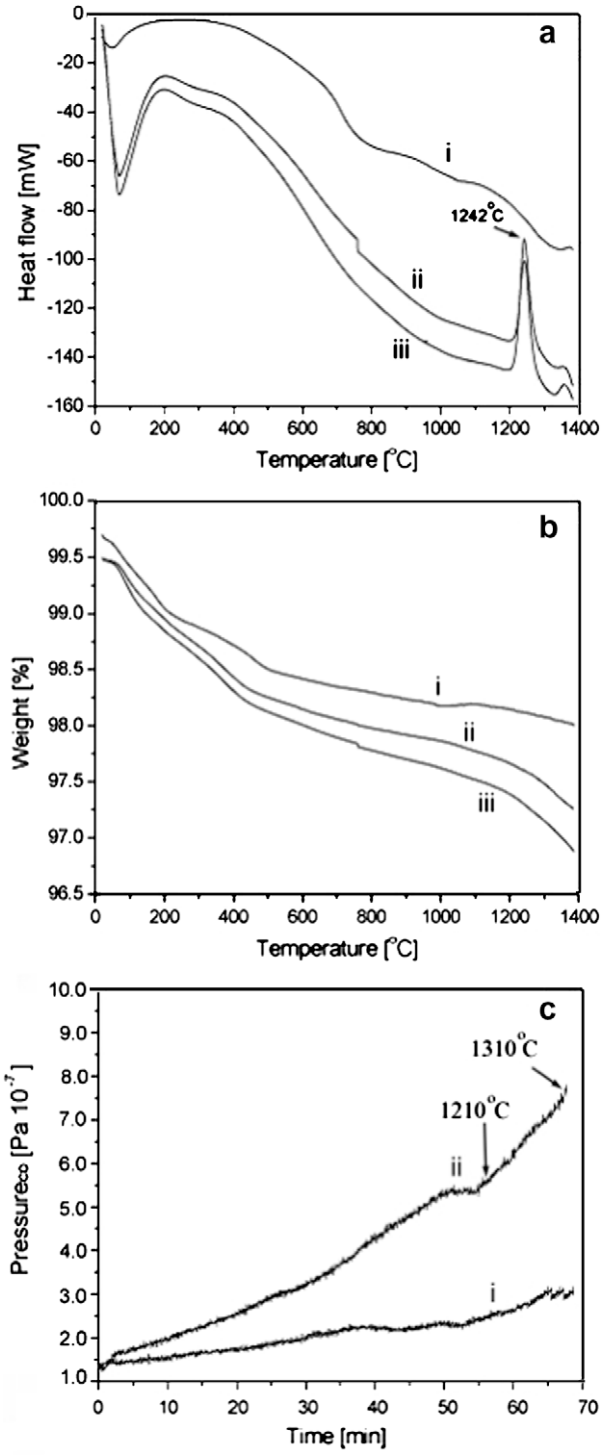

Fig. 6. (a) DTA and (b) TGA diagram for: (i) monolithic Al_2O_3, (ii) Al_2O_3–2 wt.% CNT nanocomposite, (iii) Al_2O_3–5 wt.% CNT nanocomposite; (c) mass spectrum of (i) Al_2O_3 and (ii) Al_2O_3–2 wt.% CNT nanocomposites for CO.

with the exothermic peak seen in the DTA profile, as shown in Fig. 6c.

XRD patterns of the nanocomposites show no sign of other phases except for α-Al_2O_3. Fig. 7b–d suggests that even if a new phase was formed the total amount would be extremely low, undetectable to XRD. To verify the possible formation mechanism for such new phases, a high CNT content (50 wt.%) composite powder was prepared and sintered under similar conditions. Nevertheless, except from the lower CNT contents in the nanocomposites, similar

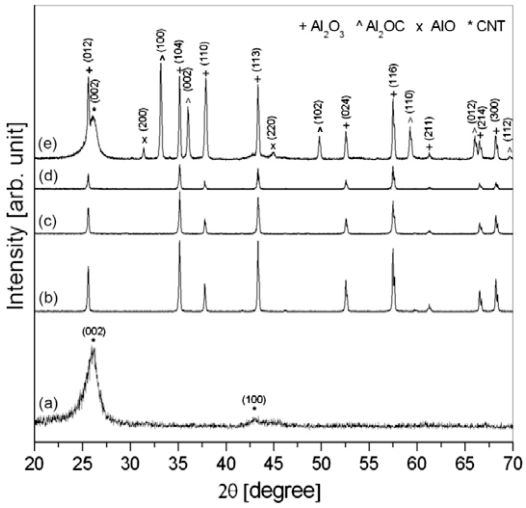

Fig. 7. XRD pattern of: (a) CNTs, (b) monolithic Al_2O_3, (c) Al_2O_3–2 wt.% CNT nanocomposite, (d) Al_2O_3–5 wt.% CNT nanocomposite, and (e) Al_2O_3–50 wt.% CNT nanocomposite.

reactions can be expected at the Al_2O_3/CNT interface. The XRD pattern has revealed the crystalline peaks of Al_2OC (JCPDS No. 00-038-0148), AlO (JCPDS No. 01-075-0278) and Al_2O_3 (JCPDS No. 01-078-2426) phase, in addition to CNTs, as shown in Fig. 7e. This result confirmed similar reactions could actually have occurred during sintering, underlining the possible reaction mechanism.

Upon heating, Al_2O_3 forms gaseous Al_2O in the presence of reducing agent carbon, whilst gaseous AlO and atomic O are the principal products when heated alone [37]. Therefore, it is likely that Al_2O_3 nanoparticles in the presence of CNTs underwent a carbothermal reduction and formed gaseous Al_2O which further reacted with the residual carbon to form Al_2OC [38]. Other studies have also described that Al_2O_3 can be reduced by carbon to form Al_4O_4C which further reacts with carbon to produce Al_4C_3 [39,40], according to the reactions described below:

$$Al_2O_3 \Longleftrightarrow 2AlO_{(g)} + O_{(g)} \quad (1)$$

$$Al_2O_3 + 2C \Longleftrightarrow Al_2O_{(g)} + 2CO_{(g)} \quad (2)$$

$$Al_2O_{(g)} + C \Longleftrightarrow Al_2OC \quad (3)$$

$$2Al_2O_3 + 3C \Longleftrightarrow Al_4O_4C + 2CO_{(g)} \quad (4)$$

$$Al_4O_4C + 6C \Longleftrightarrow Al_4C_3 + 4CO_{(g)} \quad (5)$$

However, the formation of the final compounds depends on the particle size of the starting Al_2O_3, the reaction time and temperatures. A fine particle size Al_2O_3 leads to the formation of Al_2OC; and large particle promotes the synthesis of Al_4C_3. High reaction temperatures (>1800 °C) favour the growth of Al_4C_3 and low temperatures (1500–1600 °C) result in Al_2OC [35]. A long reaction time (9 h) leads to Al_4O_4C and a short time to Al_2OC [37]. In this context, the use of Al_2O_3 nanoparticles (~40 nm) as the starting material, and the low sintering temperatures (1600 °C) and short reaction times (60 min) would all favour reactions (1) and (2) and resulted in Al_2OC. This analysis agrees well with the Al_2OC phase detected in XRD. Further, the phase marked with "×" is very difficult to identify in the XRD. It is not residue metal catalysts used for growing CNTs. It is close to the $Al_{2.4}O_{3.6}$ phase, however according to the above discussions and in the presence of reducing atmosphere, it is more likely to be AlO.

3.6. Interface reaction model

Based on the HRTEM results and the possible chemical reactions, a schematic model is proposed to explain the possible

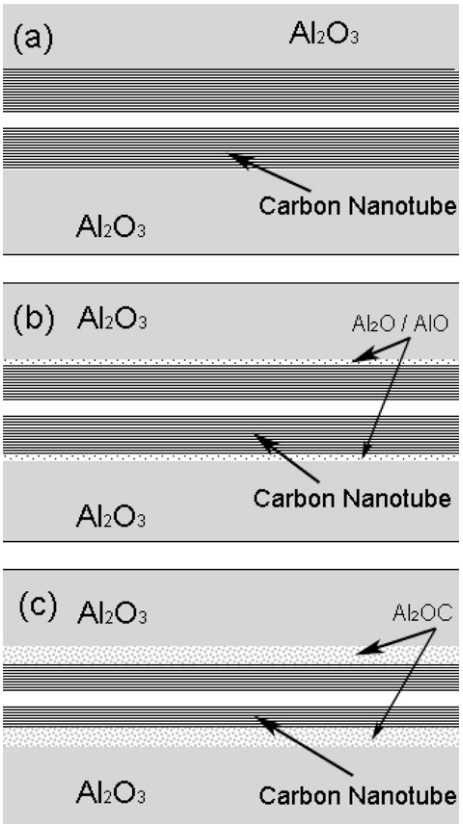

Fig. 8. A schematic model for the Al_2O_3–CNT interface.

reactions occurred at the Al_2O_3–CNTs interface, as illustrated in Fig. 8. As temperature increases, the Al_2O_3 nanopowder will react with the neighbouring outer layer of a CNT and form Al_2O or AlO sub-oxide, as shown in Fig. 8b. In the mean time, CO gas will be produced via a carbothermal reduction following reaction (2), as evidenced by the mass spectrum results. Gaseous diffusion will transport Al_2O/AlO to further react with CNT layers, which subsequently creates the Al_2OC intermediate phase following reaction (3), Fig. 8c. It is expected that the Al_2OC phase will form a thin layer sheathing the CNT and restrict the CNT from further contact or reaction with Al_2O. Hence, the carbothermal reduction of Al_2O_3 would be terminated, leaving the remaining CNT intact (without further destruction). The presence of the Al_2OC layer between CNTs and the Al_2O_3 may act as a barrier to inhibit further chemical reaction as schematically demonstrated in Fig. 8c. This seems to be verified by the fact that the CNTs maintained their original morphological and structural features in the composites, even after sintering under high temperatures and high pressures (Figs. 3a and 5a). It is believed that the Al_2O_3–CNT interface is primarily composed of Al_2OC.

The strong bonding discussed above seems to suggest that this intermediate interface is chemically compatible with both matrix and CNTs, playing an important role in the fracture toughness improvement. When the nanocomposite is ruptured, loads could be transferred effectively from the matrix to CNTs through this interfacial layer. Thus, the CNTs remain firmly bonded with the Al_2O_3 matrix and resist the pullout. They also bridged the gap of cracks and significantly contributed to the improvement of toughness and other mechanical properties.

4. Conclusions

Well-dispersed CNT-reinforced Al_2O_3 nanocomposites have been fabricated successfully with reasonably high density by hot-pressing. A 2 wt.% of CNT addition increased the hardness, flexural strength and fracture toughness of nanocomposites, however further CNT addition up to 5 wt.% slightly decreased the hardness, reduced the flexural strength but improved the toughness. The increase in mechanical properties, in particular toughness, is believed to be associated with the homogenous dispersion of CNTs within the matrix and the strong interface connections between the CNT and the matrix, which is essentially required to operate toughening mechanism. Our results confirmed the existence of an interfacial phase between the matrix and the CNTs. This Al_2OC intermediate phase was, possibly, produced via a carbothermal reduction of Al_2O_3, which appears to exhibit a good chemical compatibility with both the CNTs and the matrix. The well-dispersed CNTs within the Al_2O_3 matrix increased the pullout resistance, bridged the crack gaps and hindered the crack propagation by exploiting CNTs elasticity, leading to improved fracture toughness.

Acknowledgements

IA thanks the scholarship support from the Government of Pakistan and The University of Nottingham, United Kingdom. YZ thanks Mr. K. Dinsdale and Mr. T. Buss for their technical support.

References

[1] Mukerjee J. Ceramic matrix composites. Defence Sci J 1993;43(4):385–95.
[2] Marcin C, Katarzyna P. Processing and mechanical properties of Al_2O_3–Cr nanocomposites. J Eur Ceram Soc 2007;27:1273–9.
[3] Carroll L, Derby B. Silicon carbide size effects in alumina based nanocomposites. Acta Mater 1996;44(11):4543–52.
[4] Dupel P, Hendry A. Interfacial reaction in carbon fibre–sialon ceramic composites. J Eur Ceram Soc 1995;15:801–9.
[5] Thostenson ET, Ren Z, Chou TW. Advances in the science and technology of carbon nanotubes and their composites: a review. Compos Sci Technol 2001;61:1899–912.
[6] Treacy J, Ebbessen TW, Gibson JM. Exceptionally high Young's modulus observed for individual carbon nanotubes. Nature 1996;3(81):678–80.
[7] Ajayan M. Nanotubes from carbon. Chem Rev 1999;99:1787–99.
[8] Osayande L, Okoli OI. Fracture toughness enhancement for alumina system: a review. Int J Appl Ceram Technol 2008;5(3):313–23.
[9] Ohnabe H, Masaki S, Sasa T. Potential application of ceramics matrix composites to aero-engine components: part A. Appl Sci Manuf 1999;30:489–96.
[10] Padture NP. Multifunctional composites of ceramics and single-walled carbon nanotubes. Adv Mater 2009;21:1767–70.
[11] Sheldon BW, Curtin WA. Nanoceramics composites tough to test. Nature Mater 2004;3:505–6.
[12] Peigney A. Tougher ceramics with nanotubes. Nature Mater 2003;2:15–6.
[13] Corral EL, Garary J, Barrera EV. Engineering nanostructure for single-walled carbon nanotubes reinforced silicon nitride nanocomposites. J Am Ceram Soc 2008;91(10):3129–37.
[14] Fan J, Zhao D, Song J. Preparation and microstructure of multi-walled carbon nanotubes toughened Al_2O_3 composite. J Am Ceram Soc 2006;89(2):750–3.
[15] Yamamoto G, Omori M, Hashida T, Kimura H. A novel structure for carbon nanotube reinforced alumina composites with improved mechanical properties. Nanotechnology 2008;19:315708.
[16] Laurent C, Peigney A, Rousset A. Carbon nanotubes–Fe–Alumina nanocomposites: part II: microstructure and mechanical properties of the hot-pressed composites. J Eur Ceram Soc 1998;18:2005–13.
[17] Jinpeng F, Zhao D, Song J. Preparation and microstructure of multi-walled carbon nanotubes-toughened Al_2O_3 composites. J Am Ceram Soc 2006;89(2):750–3.
[18] Wie T, Fan Z, Wie F. A new structure for multi-walled carbon nanotubes reinforced alumina nanocomposite with high strength and toughness. Mater Lett 2008;62:641–4.
[19] Zhan G, Kuntz J, Wan J, Mukherjee K. Single-walled carbon nanotubes as attractive toughing agent in alumina based nanocomposites. Nature Mater 2003;2:38–42.
[20] Siegel RW, Chang SK, Ajayan PM, Schadler LS. Mechanical behaviour of polymer and ceramic matrix nanocomposite. Scripta Mater 2001;44:2061–4.
[21] Wang X, Padture NP, Tanaka H. Contact damage resistance ceramics/single-walled carbon nanotubes and ceramic/graphite composites. Nature Mater 2004;3:539–44.
[22] Vasiliev Alexander L, Poyota R, Padture NP. Single-walled carbon nanotubes at ceramics grain boundary. Scripta Mater 2007;56:461–3.
[23] Gao L, Jiang L, Sun J. Carbon nanotube–ceramic composites. J Electroceram 2006;17:51–5.
[24] Jinpeng F, Zhaung DM, Wu MS. Toughening and reinforcing alumina matrix composite with single-walled carbon nanotubes. Appl Phys Lett 2006;89:121910.

[25] Pippel E. Structure, composition and function of interfaces in ceramics fibre/matrix composites. J de Physique 1993;3:1905–10.
[26] Sababalázsi C, Sedláčková K, Czigány Z. Structural characterization of Si_3N_4–carbon nanotube interfaces by transmission electron microscopy. Compos Sci Technol 2008;68:1596–9.
[27] Ajayan PM. Nanotubes from carbon. Chem Rev 1999;99:1787–99.
[28] Anstis GR, Chantikul P, Marshall DB. A critical evaluation of indentation technique for measuring fracture toughness: I. Direct crack method. J Am Ceram Soc 1981;64(9):533–8.
[29] ASTM E399. Standard test method for plain strain fracture toughness of metallic materials, Annual book of ASTM standards, V.03.01. ASTM, Philadelphia, USA; 1991.
[30] Shen TK, Hing P. Ultrasonic through-transmission method of evaluating the modulus of elasticity of Al_2O_3–ZrO_2 composite. J Mater Sci 1997;32:6633–8.
[31] Quinn GD, Bradt RC. On the vickers indentation fracture toughness test. J Am Ceram Soc 2007;90(3):673–80.
[32] Ahmad I, Kennedy A, Zhao Y, Zhu YQ. Carbon nanotubes reinforced MgO-doped Al_2O_3 nanocomposites. In: Proceeding of ECCM13: 13th European conference on composite materials, Stockholm, Sweden; 2008.
[33] Bengisu M. Engineering ceramics. Berlin: Springer-Verlag; 2001. p. 227 [chapter 4].
[34] An W, Lim DS. Effect of carbon nanotube additions on the microstructure of hot-pressed alumina. J Ceram Process Res 2002;3:201–4.
[35] Kim BN, Wakayama S, Kawahara M. Characterization of 2-dimensional crack propagation behaviour simulation and analysis. Int J Fract 1996;75:247–59.
[36] Ahmad I, Cao H, Chen H, Zhao H, Kennedy A, Zhu YQ. Carbon nanotube toughened aluminium oxide nanocomposites. J Eur Ceram Soc 2009;30:865–73.
[37] Brewer L, Searcy AWJ. The gaseous species of Al–Al_2O_3 system. J Am Chem Soc 1951;73(11):5308–13 .
[38] Cox JH, Pidgeon LM. An investigation of the aluminium–oxygen–carbon system. Can J Chem 1963;41:671–83.
[39] Zhao J, Lin W, Yamaguchi A, Ommyoji J, Sun J. Influence of heating temperature, keeping time and raw materials grain size on Al_4O_4C synthesis in carbothermal reduction process and oxidation of Al_4O_4C. J Ceram Soc Jpn 2007;115:654–60.
[40] Stroup PT. Carbothermal smelting of aluminium. Trans Metall Soc AIME 1964;230:356–72.